IEEE Access
Multidisciplinary | Rapid Review | Open Access Journal

SPECIAL SECTION ON NEW TRENDS IN BRAIN SIGNAL PROCESSING AND ANALYSIS

Received November 8, 2018, accepted November 17, 2018, date of publication November 26, 2018,
date of current version December 27, 2018.

Digital Object Identifier 10.1109/ACCESS.2018.2882860

A New Optical Information Processing Device Design for Internet of Brain Things Application

CHUNLI WANG[1], YONGSHUN WANG[1], AND HONGYI LI[2,3]

[1]School of Electronic and Information Engineering, Lanzhou Jiaotong University, Lanzhou 730070, China
[2]Xinjiang Quality of Products Supervision & Inspection Institute of Technology, Ürümqi 830011, China
[3]Xinjiang Technical Institute of Physics & Chemistry, Chinese Academy of Sciences, Ürümqi 830011, China

Corresponding author: Hongyi Li (lihy@ms.xjb.ac.cn)

This work was supported by the National Natural Science Foundation of China under Grant 61366006 and Grant 61461024.

ABSTRACT With the development and application of Internet of things, new requirements for optical communication technology are put forward, and this text proposed new optical information processing device design logic-oriented-based for Internet of brain things application. Three micro rings were coupled with three different shapes of optical waveguide components, their wavelengths were varied with the change of the applied voltages (logical input) so as to control the propagation direction of the input optical signal and the final output forms of lighting or darkness representing different logic level values as the result of the logical operations. The working wavelength of the device was determined as 1.5146 μm through static simulations with MATLAB tools, and it was proved that the functions of flexible optical switch logic operations ''and/not'', ''or/nor'', and ''xor/xnor'' can be realized in the dynamic simulations, the results indicated that the device with low-power consumption, high-bandwidth, flexible structure, and multiple logical operation functions has been accomplished and can be used as components of VLSI designs in future. This paper also gives a useful reference to many Internet of brain things applied field.

INDEX TERMS Electro-optical logic gate, Internet of brain things, logical operation, micro ring resonator.

I. INTRODUCTION

Communication technology is one of the important technologies in the transport layer of the Internet of things. With the development of the new generation information technology, the Internet of brain things technology has been widely applied. At the same time, higher requirements for optical communication technology are put forward. For example, in recent years, under the requirement of miniaturization, integration and high-speed processing, the micro ring resonator (MRR) formed by a closed loop waveguide coupled with a straight one is widely used in the fields of weapon equipment, environmental monitoring, disease diagnosis and so on owing to its mature technology and high integration of optoelectronic [1]. Rabus has put forward a race tracker ring resonator transverse multi-coupled made of an integrated semiconductor optical amplifier (SOA) with the tuned filter function. Grover adopted a new method which a vertical coupled micro ring resonator and a frequency separation filter were realized in the GaInAs P-InP material system. Ibrahim has made an all-optical switch with single micro ring resonator used in the time-division multiplex data transmission channel, with approximately 8 decibels crosstalk in space. However, any transmission intensity in any number of channels can not be controlled, therefore, these structures were not flexible enough in terms of applications in optical switch or optical filter. In this paper, multiple micro ring resonators coupled with different shapes of optical waveguides and the modulated characteristic of the refractive index of electro-optic polymer materials applied, the optical logic-oriented device with different logic operation functions was designed and realized. This device has the features of compact structures, low power consumptions and flexible control of the input and output.

The concept of logic-oriented was a principle of Boolean logic operation proposed by American scientist James Hardy and Israeli scientist Joseph Shamir in 2007. The switch states and directions of the light propagation in the optical network are controlled by logic operands, moreover, the results of the logic operation are output in the form of light at the specific ports [2], [3], accordingly, a method of optical processing logic-oriented-based is studied and a multifunctional electro-optical logic gate device has been designed and realized in this paper.

The paper structure is as follows. Section 2 first analyzes Design of logic-oriented-based device for Internet of brain things communication layer. Section 3 presents the Design

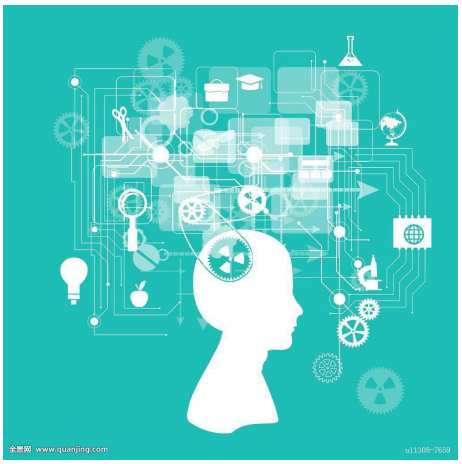

FIGURE 1. Various connection logic for the Internet of brain things.

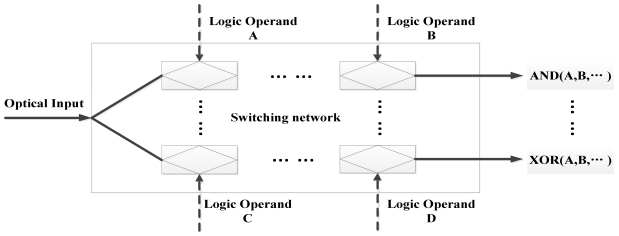

FIGURE 2. Principle diagram of the optical switches logic-oriented.

method of switching logic devices based on the micro-ring resonator. Section 4 reports the Static simulation of the multi-functional electro-optical logic device function under IOT. Section 5 reports the logic function dynamic simulation of the optic-oriented device and its IOT application.

II. DESIGN OF LOGIC-ORIENTED-BASED DEVICE FOR INTERNET OF BRAIN THINGS COMMUNICATION LAYER

A. INTERNET OF BRAIN THINGS COMMUNICATION CONNECT AND OPTICAL LOGIC-ORIENTED

Communication connection technology is one of the core technologies in the application of Internet of brain things, Figure.1 shows various connection logic of the Internet of brain things. As we known, Design of logic-oriented-based device is a key technology of optical communication application. The logic operands of the logic-oriented device are represented the temperature field, electric field or light field. The optical input manipulated by different logic operands can be guided to different output as the results of different logic operations [4], [5]. Furthermore, some complex combinational logic operations can also be achieved by designing different switching circuits as indicated in Figure.2.

Due to its linear propagation in the logic-oriented device, the manufacturing processes of the devices are simple, and logical operation function is easy to achieve [6]. The micro ring polymer-based consists of three parts, as shown in Figure.2, The core of electro-optics waveguide with the refractive index of n_1, the loss factor of α_1 and the thickness of b_1, is a kind of material polymer-based with the effect of electro-optics. The neighbor upper and lower buffer layers with the refractive index of n_2, the loss factor of α_2 and thickness of b_2, and the upper and lower electrodes with the refractive index of n_3, the amplitude transfer factor of k_3 and thickness of b_3 are both non-polarized polymer-based material, therefore, n_2 and n_3 will not vary with the applied voltages.

The temperature of the electro-optic material was varied with the applied voltages U on the upper and lower electrodes firstly, then the effective refractive index of the electro-optic waveguide core material was changed and modulated by the thermo-optic effect of this polymer material, at the same time, the wavelength of the input optical signal was blue shifted or red shifted representing the switch states of "on/off" and output as the results of logical operations. Different optical circuit structures logic-oriented-based with different logical operation functions can also be designed applying multiple micro rings polymer-based coupled with different shapes of optical waveguides. A variety of optical switch logic operations such as and/or, or/nor and xor/xnor can be completed by modifying the logic input of different ports.

B. THE ELECTRO-OPTIC PROPERTIES OF THE POLYMER-BASED

The property of the electro-optic polymer-based is studied using the main axis O-XYZ coordinate system applied voltages for the electro-optical modulation. It is assumed that the polymeric material has been polarized in the direction of its thickness and this polarized direction is set as axis z [7]. The polarized polymer material has the characters of anisotropic and the effect of electro-optic. The electrode structure, as shown in Figure.3, is symmetrical and each distribution $E_y(x,y)$ of the electric field along the axis y caused by the modulation voltage U was expressed as:

$$E_y(x, y) = E_{1y} + E_{2y}(x, y) + E_{3y}(x, y) \tag{1}$$

Where, E_{1y} represents a uniform electric field between the upper and lower electrodes, the non-uniform fields $E_{2y}(x, y)$ and $E_{3y}(x, y)$ formed by the two upper and lower surface electrodes may be neglected due to its weakness. E'_{1y} represents electric field in the buffer layer. By applying the continuity

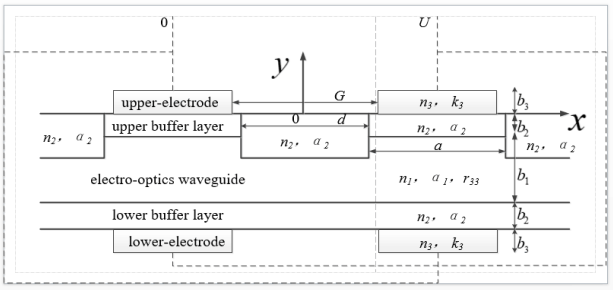

FIGURE 3. Diagram of cross section of waveguide in an electro-optical coupled area.

TABLE 1. Working wavelength in the non-resonant area.

	Download port	Pass-through port
Working wavelength in the non-resonant area	0	-40dB
	Logic“1”	Logic“0”
	-60dB	0
High-level voltage	Logic“0”	Logic“1”

TABLE 2. Working wavelength in the resonant area.

	Download port	Pass-through port
Working wavelength in the resonant area	-60dB	0
	Logic“0”	Logic“1”
	0	-38dB
Low-level voltage	Logic“1”	Logic“0”

conditions $n_1^2 E_{1y} = n_2^2 E'_{1y}$ of the electric displacement at the interface of the dielectric layer and the relationship $U = E_{1y} b_1 + 2E'_{1y} b_2$ between the applied voltage and electric fields, the uniform electric field E_{1y} in waveguide core was deduced as equation (2).

$$E_{1y} = \frac{n_2^2 U}{2n_1^2 b_2 + n_2^2 b_1} \tag{2}$$

Accordingly, the refractive index change of the electro-optic material with the electro-optic coefficient r_{33} in the waveguide core was described as equation (3).

$$\Delta n_1 = \frac{1}{2} n_1^3 r_{33} E_{1y} = \frac{n_1^3 n_2^2 r_{33} U}{2(2n_1^2 b_2 + n_2^2 b_1)} \tag{3}$$

Since the buffer layer in the waveguide is a kind of non-electro-optic material, the refractive indexes n_2 and n_3 will not vary with the applied electric field.

C. OPERATING MODES OF MULTI-FUNCTIONAL ELECTRO-OPTICAL LOGIC DEVICES BASED ON POLYMER

The same as the “positive logic” and “negative logic” applied in digital circuits, the working wavelength in the resonant or non-resonant area is a dual operating mode in the optical logic-oriented [8]. The working wavelength is determined by the spectral response at the downloading port after the broadband light of different wavelength is input to the logic circuit, furthermore, the operating mode and the modulation voltage can be gotten.

The first one is in a high-level voltage with its wavelength in the non-resonant area, similar to the “positive level” in the electrical logic. The second one is in a low-level voltage with the wavelength in the resonant area, similar to the “negative level” in the electrical logic as summarized in Table 1, 2 above.

III. DESIGN OF SWITCHING LOGIC DEVICES BASED ON THE MICRO-RING RESONATOR

The structure of the switch logic device based on the micro ring resonator is shown in Figure.4. It consists of three micro rings coupled with a straight, a U-shaped and a curved waveguide. The varied voltages applied on Ring1, Ring2 and Ring3 are used as logic input of this device and the real optical signal input is output to the ports of Output1, Output2 or Output3 as the result of different logic operations such as and/or, or/nor and xor/xnor.

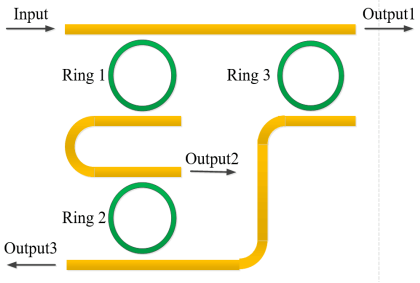

FIGURE 4. Diagram of the device structure.

It is presumed that all of the amplitude transfer factors k in the corresponding coupled area of three annular waveguides are the same, then the corresponding amplitude transmission factor t is the same too. Assuming that the radius of the micro ring is R, the corresponding coupled area can be expressed as:

$$\begin{bmatrix} A_2 \\ B_2 \end{bmatrix} = \begin{bmatrix} \frac{t}{jk} & -\frac{1}{jk} \\ \frac{1}{jk} & -\frac{t}{jk} \end{bmatrix} \begin{bmatrix} A_1 \\ B_1 \end{bmatrix},$$

$$\begin{bmatrix} C_1 \\ D_1 \end{bmatrix} = \begin{bmatrix} \frac{t}{jk} & -\frac{1}{jk} \\ \frac{1}{jk} & -\frac{t}{jk} \end{bmatrix} \begin{bmatrix} C_2 \\ D_2 \end{bmatrix},$$

$$\begin{bmatrix} E_2 \\ F_2 \end{bmatrix} = \begin{bmatrix} \frac{t}{jk} & -\frac{1}{jk} \\ \frac{1}{jk} & -\frac{t}{jk} \end{bmatrix} \begin{bmatrix} E_1 \\ F_1 \end{bmatrix} \tag{4}$$

$$\begin{bmatrix} G_1 \\ H_1 \end{bmatrix} = \begin{bmatrix} \frac{t}{jk} & -\frac{1}{jk} \\ \frac{1}{jk} & -\frac{t}{jk} \end{bmatrix} \begin{bmatrix} G_2 \\ H_2 \end{bmatrix},$$

$$\begin{bmatrix} I_2 \\ J_2 \end{bmatrix} = \begin{bmatrix} \frac{t}{jk} & -\frac{1}{jk} \\ \frac{1}{jk} & -\frac{t}{jk} \end{bmatrix} \begin{bmatrix} I_1 \\ J_1 \end{bmatrix},$$

$$\begin{bmatrix} K_1 \\ L_1 \end{bmatrix} = \begin{bmatrix} \frac{t}{jk} & -\frac{1}{jk} \\ \frac{1}{jk} & -\frac{t}{jk} \end{bmatrix} \begin{bmatrix} K_2 \\ L_2 \end{bmatrix} \tag{5}$$

Supposing the bend loss of the micro ring is α_R,the rules of light transmission in these three micro rings are shown as

the following equations(6-8).

$$\begin{bmatrix} C_2 \\ D_2 \end{bmatrix} = \begin{bmatrix} 0 & \exp(-j\phi) \\ \exp(j\phi) & 0 \end{bmatrix} \begin{bmatrix} A_2 \\ B_2 \end{bmatrix} \quad (6)$$

$$\begin{bmatrix} G_2 \\ H_2 \end{bmatrix} = \begin{bmatrix} 0 & \exp(-j\phi) \\ \exp(j\phi) & 0 \end{bmatrix} \begin{bmatrix} E_2 \\ F_2 \end{bmatrix} \quad (7)$$

$$\begin{bmatrix} K_2 \\ L_2 \end{bmatrix} = \begin{bmatrix} 0 & \exp(-j\phi) \\ \exp(j\phi) & 0 \end{bmatrix} \begin{bmatrix} I_2 \\ J_2 \end{bmatrix} \quad (8)$$

Where, the phase factor is calculated by the formula $\phi = \pi R(\beta\text{-}j\alpha_R)$ and the mode transfer coefficient is obtained by the formula $\beta = 2\pi n_{eff}/\lambda$.

At the same time, it is assumed that the bend loss in the waveguide connected to MRR1 and MRR2 is α_1 and α_2 respectively. Ignoring the loss of straight waveguide, the performance of the optical signal transmission is derived from the following equations:
Between MRR1 and MRR3:

$$I_1 = B_1 \quad (9)$$

Between MRR1 and MRR3:

$$E_1 = \exp(-j\pi R(\beta - j\alpha_1))D_1 \quad (10)$$

Between MRR3 and MRR2:

$$G_1 = \exp(-j\pi R(\beta - j\alpha_2))L_1 \quad (11)$$

According to the above relationships, the normalized output light field intensity of the three output ports relative to the input port can be deduced. In this paper, the device with the polarized electro-photopolymer material with the electro-optic coefficient r_{33} has the character of the first-order linear electro-optic effect [10] and its refractive index described in the following equation (12) varies with the applied voltages U [11].

$$\Delta n_1 = \frac{1}{2} n_1^3 r_{33} E_1 = \frac{n_1^3 n_2^2 r_{33} U}{2(2n_1^2 d_2 + n_2^2 d_1)} \quad (12)$$

Hence the modified effective refractive index is represented by equation (13):

$$n_{eff} = n_1 + \Delta n_1 \quad (13)$$

Where, U is the voltage applied on the electrodes, n_2 and n_3 are the refractive indexes of the buffer layers and electrodes made from the non-polarized polymeric material, which will not vary with the applied voltages U. The logic operation functions of optical switches can be realized by the blueshift or redshift of the micro ring resonant wavelength caused by the variation of the applied voltages.

IV. STATIC SIMULATION OF THE MULTI-FUNCTIONGAL ELECTRO-OPTICAL LOGIC DEVICE FUNCTION UNDER IOT

According to the mathematical model, the static performances of the electro-optical logic gate device were simulated in Matlab software [32]–[34]. The set device parameters were listed in Table 3. A horizontal axis is represented as the logic voltages input to the micro rings and the vertical axis is shown as the output spectrum based on the results of different logic operations.

According to equation (12), when U is equal to 51.8V, the change of refractive index of the electro-optic polymer is 0.001. Broadband light with different wavelengths is input

TABLE 3. Table of setting parameters in the simulations.

Parameters in the simulations	Values
Coupled distance between the straight waveguide and the micro ring	$0.23\mu m$
Amplitude coupled factor of k	0.1
Bend radius of the micro ring of R	$10\mu m$
Bend loss of the micro ring α_R	$0.25dB/km$
Refractive index n_2 of the buffer layer	1.461
Thickness $d_1$of the core waveguide in the micro ring	$1.7\mu m$
Thickness $d_2$of the buffer layer in the micro ring	$2.5\mu m$
Effective refractive index	1.59
Electro-optic coefficient of r_{33}	$68pm/V$
Relations of coupled factor k and amplitude transfer factor t	$k^2+t^2=1$

TABLE 4. Applied voltages and the corresponding output spectrums of each micro-ring.

	Ring1	Ring 2	Ring 3	Output Spectrum
Load Voltage/ V	0	0	0	Figure.5 (a)
	0	0	51.8	Figure.5 (b)
	0	51.8	0	Figure.5 (c)
	0	51.8	51.8	Figure.5 (d)
	51.8	0	0	Figure.5 (e)
	51.8	0	51.8	Figure.5 (f)
	51.8	51.8	0	Figure.5 (g)
	51.8	51.8	51.8	Figure.5 (h)

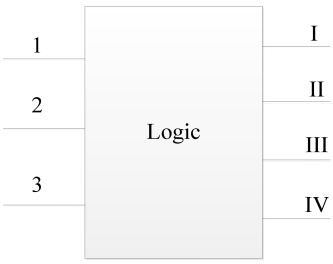

FIGURE 5. Diagram of the input and output of the logic gate.

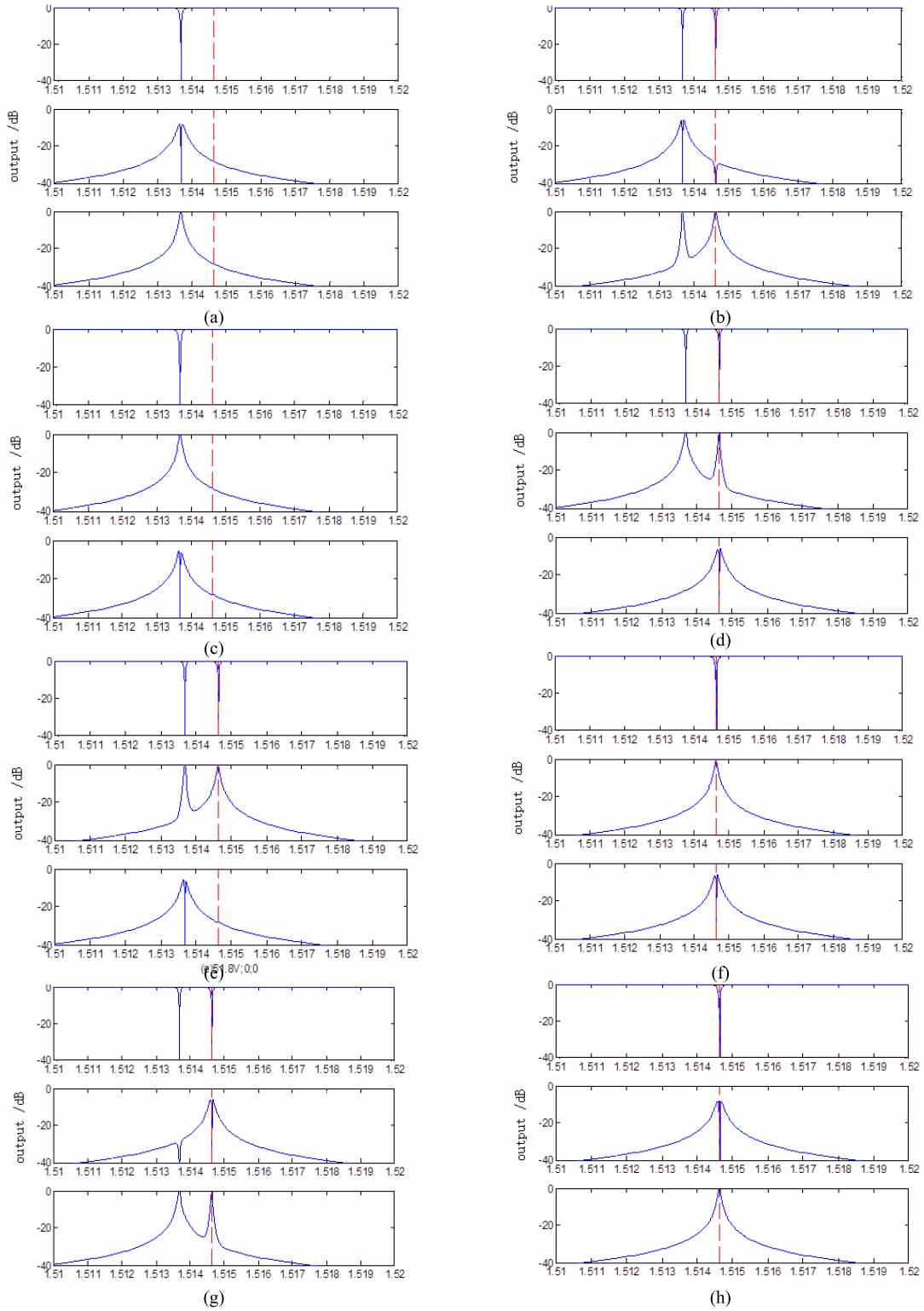

FIGURE 6. Diagrams of output spectrums of micro ring R1, R2, R3 applied with different voltages.

to this device, the logic voltage and normalized output spectrums corresponded are summarized below in Table 4 by changing the modulation voltage states of these three micro-rings.

As a logic gate of the logic circuit described in Figure.5, the corresponding relations between the logic output and the real ports of this device are logic output I corresponded to Output2, logic output II corresponded to Output3, logic

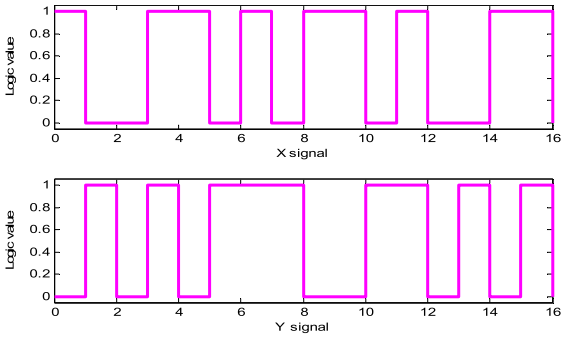

FIGURE 7. The modulated signals applied to the MRR.

output III corresponded to Output1 and logical output IV corresponded to Output1 plus Output3. A number of logical operation results can be achieved at the different ports by changing the logic input [35]–[39].

Compared with the ways of output shown in Figure.6 (a-h), the resonant peak-wavelength 1.51463 μm is tested and determined as the working wavelength. In the first working pattern, it is defined as a high-level with the control voltage 51.8V on the micro ring as logic "1" and a low-level *0V* as logic "0". If there is no voltage applied on the micro ring or the logic input is "000", the normalized light intensity output to Output1, Output2 and Output3 is-28.89dB,-28.87dB and 0dB respectively, which is defined as the logical "001". In the same way, the logical values of the normalized output light intensity corresponding to the different logic input can be obtained in the condition of the working wavelength [40]–[44].

V. THE LOGIC FUNCTION DYNAMIC SIMULAITON OF THE OPTIC-ORIENTED DEVICE AND ITS IOT APPLICAITONS

A high-level voltage *51.8V* and a low-level *0V* applied to the MRR are defined as logic "1" and logic "0" separately. Dynamic simulation experiments based on Matlab software were done and two kinds of modulated signals shown in Figure.7 are used as the logic input.

A. IMPLEMENTATION OF THE LOGIC OPERATIONS AND/NOT

X signal is applied to MRR1 and MRR3 and *y* signal to MRR2. The output signals of ports II and III are shown in Figure.8 (a) and (b). The normalized output intensity below the threshold of 0.2 and above the threshold of 0.8 is defined as logic "0" and logic "1", then the output of the logic signals are shown in Figure.8 (c) and (d).

Comparing the input signals *x* and *y* and analyzing the logic outputs of ports II and III, conclusions are drawn as the follows:

1) When the input is all of "1", the output of port II is logic "1", if there is one logic "0" between the input signals *x* and *y*, logic "0" is the output, the algorithm of the AND operation is satisfied.
2) The logical output corresponding to port III is reciprocal to the logical value of the input signal *x*. The algorithm of the NOT operation is realized.

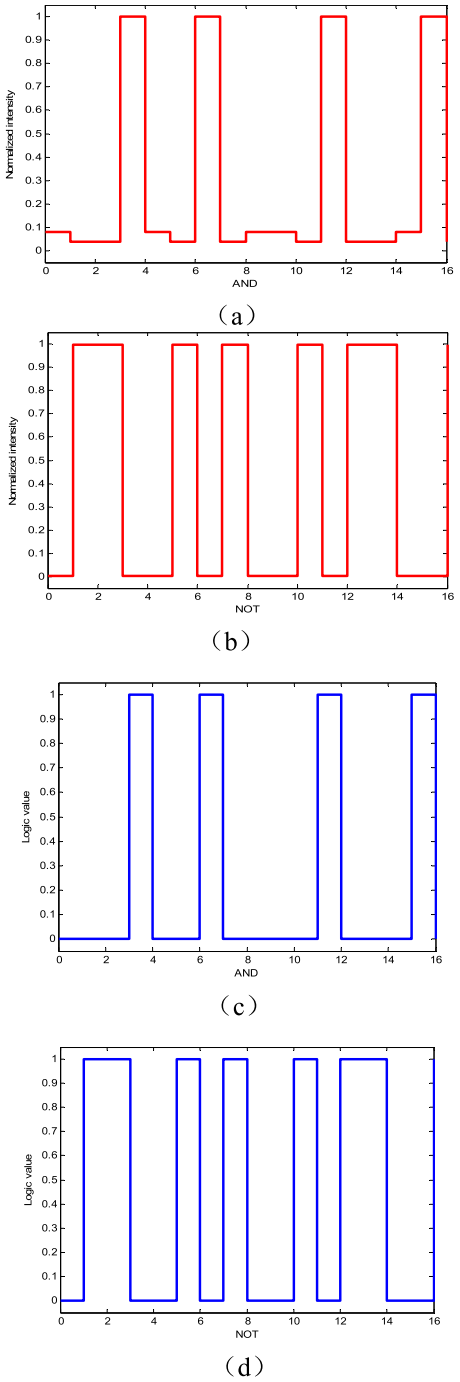

FIGURE 8. Simulation results of logic operations of AND And NOT (a) Logic operation of AND at port II. (b) Logic operation of NOT at port III. (c) Logic values of AND (d) Logic values of NOT.

Above all, logic functions of AND and NOT of this device can be achieved.

B. IMPLEMETNTAITON OF THE LOGIC OPERATIONS OR/NOR

X signal is applied to MRR1 and MRR2 and *y* signal to MRR3. The output signals of ports II and III are shown in Figure.8 (a) and (b). Similarly, the normalized output intensity below the threshold of 0.2 or above the threshold of 0.8 is

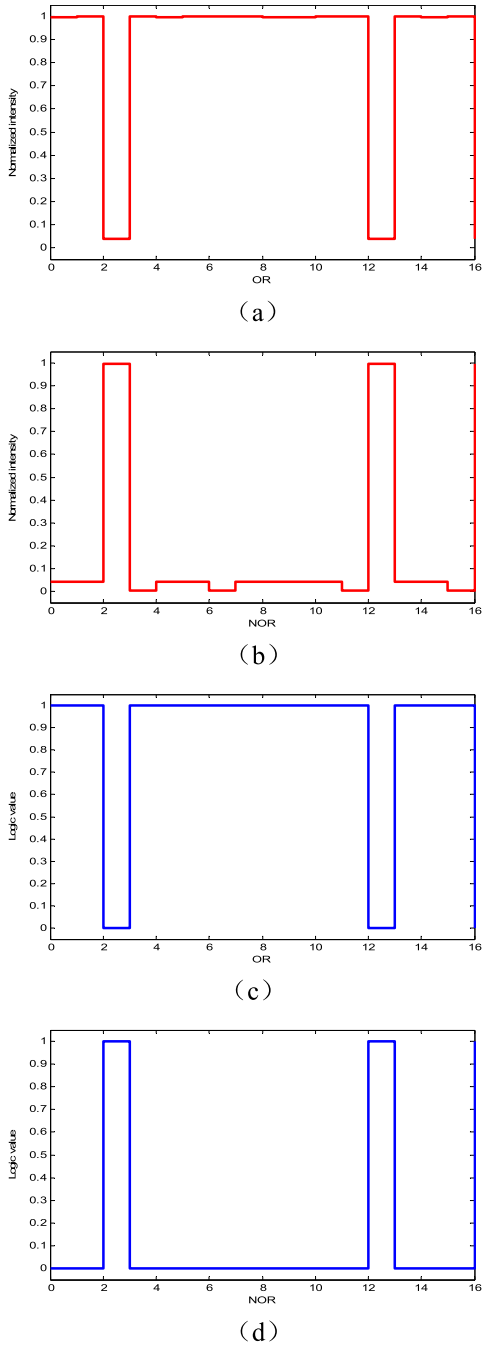

FIGURE 9. Simulation results of logic operations OR and NOR (a) Logic operation of OR at port II. (b) Logic operation of NOR at port III. (c) Logic values of OR. (d) Logic values of NOR.

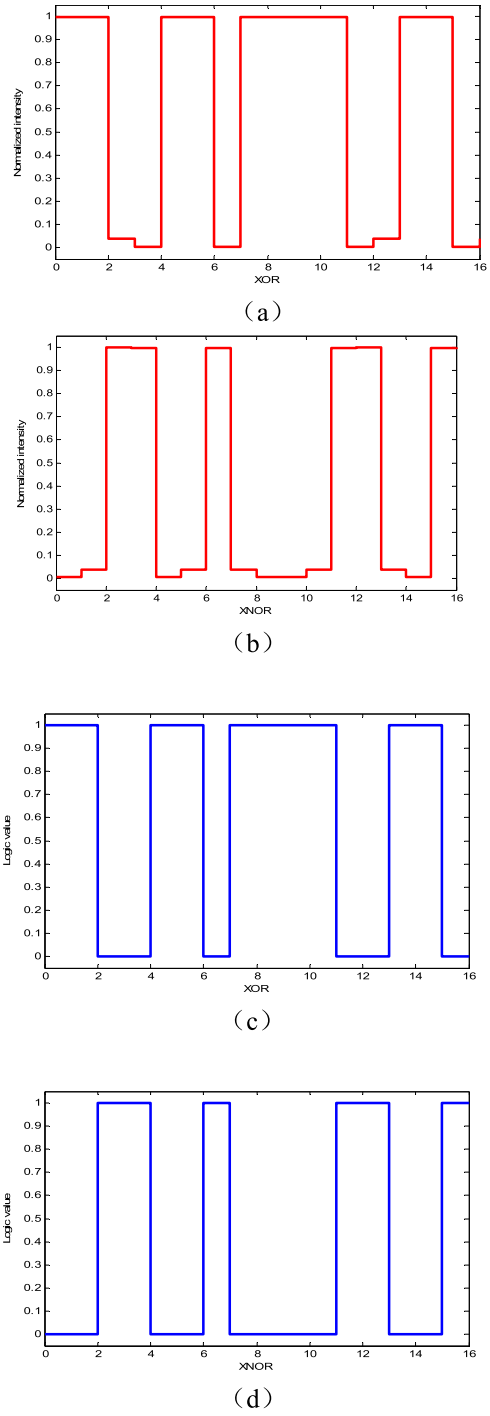

FIGURE 10. Simulation results of logic operations XOR and XNOR (a) Logic operation of XOR at port I. (b) Logic operation of XNOR at port IV. (c) Logic values of XOR. (d) Logic values of XNOR.

defined as logic "0" or logic "1", then the output of the logic signals are shown in Figure.9 (c) and (d).

Comparing the input signals x and y and analyzing the logic outputs of ports II and III, conclusions are drawn as the follows:

1) When the input is all of "0", logic "0" is the output of port II, if there is one logic "1" between the input signals x and y, logic "1" is the output, the algorithm of OR operation is satisfied.

2) When the input is all of "0", logic "1" is the output of port III, if there is one logic "1" between the input signals x and y, logic "0" is the output, the algorithm of the NOR operation is satisfied.

Above all, logic functions of OR and NOR of this device can be achieved.

C. XOR/XNOR LOGIC OPERATIONS WITH IOT APPLICATIONS

The truth table of the logic operations XOR and XNOR are shown in Table 5. x signal is applied to MRR1 and y signal

TABLE 5. The truth table of logic operations XOR/XNOR.

Logic operation of XOR			Logic operation of XNOR		
Input X	Input Y	Output Z	Input X	Input Y	Output Z
0	0	0	0	0	1
0	1	1	0	1	0
1	0	1	1	0	0
1	1	0	1	1	1

FIGURE 11. Internet of brain things application with optical communication technology.

to MRR2 and MRR3, the output signals of ports I and IV are shown in Figure.10 (a) and (b). Similarly, the normalized output intensity below the threshold of 0.2 or above the threshold of 0.8 is defined as logic "0" or logic "1", then the output logic signals are shown in Figure.10 (c) and (d).

Compared with the input signals x and y, and analyzing the logic outputs of ports I and IV, conclusions are drawn as the follows:

1) When the input logic is same, logic "0" is the output of port I, while the input logic is different, logic "1" is the output of port I, the algorithm of the XOR operation is satisfied.

2) When the input logic is same, logic "1" is the output of port IV, while the input logic is different, logic "0" is the output of port IV, the algorithm of the XNOR operation is satisfied.

Above all, logic functions of NOR and XNOR of this device can be achieved. And now Internet of things with optical communication technology used in many field [45]–[49], shown as in Figure.11.

VI. CONCLUSIONS

Compared with the characteristics of inorganic electro-optical materials, the polarized polymer material has the features of the higher electro-optical coefficient, easier to adjust the refractive index, faster response and lower threshold of switching voltage. In this paper, Multi-functional electro-optical logic gate applied this polarized polymer-based material is designed and modulated by the change in the refractive index. The working wavelength of this device is determined by the static simulation and a variety of the logic operations based on the different states of optical switch such as and/or, or/nor and xor/xnor is realized respectively with the variation of different logic input by the dynamic simulation. It is proved this device has the function of high-speed and efficient logic operations. This design method also give a useful reference to many IOT research and applied field [50]–[60], especially for Internet of brain things field.

ACKNOWLEDGMENT

Authors wish to thank NSFC under which the present work was possible.

REFERENCES

[1] L. Yi, X. Deng, M. Wang, D. Ding, and Y. Wang, "Localized confident information coverage hole detection in Internet of Things for radioactive pollution monitoring," *IEEE Access*, no. 5, pp. 18665–18674, 2017.
[2] F. Anjomshoa, M. Aloqaily, B. Kantarci, M. Erol-Kantarci, and S. Schuckers, "Social behaviometrics for personalized devices in the Internet of Things era," *IEEE Access*, vol. 5, pp. 12199–12213, May 2017.
[3] Y. Yunji, "Study of delay line based on polymer planar optical waveguide," M.S. thesis, Dept. Electron. Eng., Jilin Univ., Jilin, China, 2009.
[4] Z. Fanfan, Z. Lei, and Y. Lin, "Optical oriented logic devices silicon-based micro-ring resonators," *Adv. Laser Optoelectron.*, vol. 52, no. 11, pp. 28–37, 2014.
[5] W. Rui, "Analysis of optoelectronic switch based on polarized polymer integrated waveguide," Ph.D. dissertation, Dept. Elect. Eng., Jilin Univ., Jilin, China, 2012.
[6] X.-J. Li, R. Wu, Y.-F. Hu, L.-X. Hu, and J.-C. Guo, "Study of energy transfer in silicon-based micro-ring resonators," *Optoelectron. Lett.*, vol. 10, no. 5, pp. 321–324, 2015.
[7] M. Yang *et al.*, "Non-blocking 4×4 electro-optic silicon switch for on-chip photonic networks," *Opt. Express*, vol. 19, no. 1, pp. 47–54, 2011.
[8] L. Shiyun, I. Yasuhiko, and W. Kazumi, "Demonstration of optical computing logics based on binary decision diagram," *Opt. Express*, vol. 20, no. 2, pp. 1378–1384, 2012.
[9] L. Yi *et al.*, "All-optical switch of silicon-based dual micro-ring resonator cascaded based on thermal nonlinearity," *China Laser*, vol. 40, no. 2, pp. 164–170, 2013.
[10] R. Guanghui, C. Shaowu, and C. Tongtong, "Theoretical analysis of a tunable thermo-optic micro-loop filter cascaded," *Phys. Lett.*, vol. 61, no. 3, pp. 233–239, 2012.
[11] Z. Yao *et al.*, "An advanced development of all-optical logic gate nano-waveguide-based," *J. Elementary Technol.*, vol. 39, no. 2, pp. 130–135, 2015.
[12] Z. Xin, L. Zhiquan, and T. Kai, "High speed functional electro-optical logic based on multiple micro-rings cascaded," *J. Optoelectron. Laser*, vol. 25, no. 11, pp. 2053–2059, 2014.
[13] N. Q. Ngo, S. F. Yu, S. C. Tjin, and C. H. Kam, "A new theoretical basis of higher-derivative optical differentiators," *Opt. Commun.*, vol. 230, nos. 1–3, pp. 115–129, 2014.
[14] M. Kulishov and J. Azaña, "Long-period fiber gratings as ultrafast optical differentiators," *Opt. Lett.*, vol. 30, no. 20, pp. 2700–2702, 2015.
[15] N. K. Berger, B. Levit, B. Fischer, M. Kulishov, D. V. Plant, and J. Azaña, "Temporal differentiation of optical signals using a phase-shifted fiber Bragg grating," *Opt. Express*, vol. 15, no. 2, pp. 371–381, Jan. 2007.
[16] F. Liu *et al.*, "Compact optical temporal differentiator based on silicon microring resonator," *Opt. Express*, vol. 16, no. 20, pp. 15880–15886, 2017.
[17] Y. Haidong *et al.*, "Temporal differentiator using a twin-core fiber," *Opt. Eng.*, vol. 52, no. 1, pp. 15005–15013, 2013.
[18] H. Shahoei, D.-X. Xu, J. H. Schmid, and J. Yao, "Photonic fractional-order differentiator using an SOI microring resonator with an MMI coupler," *IEEE Photon. Technol. Lett.*, vol. 25, no. 15, pp. 1408–1411, Aug. 1, 2013.
[19] J. Dong *et al.*, "Photonic Hilbert transformer employing on-chip photonic crystal nanocavity," *J. Lightw. Technol.*, vol. 32, no. 20, pp. 3704–3709, Oct. 15, 2014.

[20] X. Yan, C.-S. Ma, X.-Y. Wang, D.-M. Zhang, and S.-Y. Liu, "Optimum design of a polymer electro-optic microring resonator switch," *Optoelectron. Lett.*, vol. 3, no. 6, pp. 423–427, 2017.
[21] X. Yan, C.-S. Ma, C.-T. Zheng, X.-Y. Wang, and D. M. Zhang, "Analysis of polymer electro-optic microring resonator switches," *Opt. Laser Technol.*, vol. 42, no. 3, pp. 526–530, 2015.
[22] C.-T. Zheng, C.-S. Ma, X. Yan, X.-Y. Wang, and D.-M. Zhang, "Analysis of response characteristics for polymer directional coupler electro-optic switches," *Opt. Commun.*, vol. 281, no. 24, pp. 5998–6005, 2015.
[23] K. Sun *et al.*, "All-optical logic gates (XOR, AND, and OR) based on cross phase modulation in a highly nonlinear fiber," *IEEE J. Opt. Commun.*, vol. 22, no. 6, pp. 1199–1201, Jun. 2009.
[24] J. Dong, X. Zhang, and D. Huang, "A proposal for two-input arbitrary Boolean logic gates using single semiconductor optical amplifier by picosecond pulse injection," *Opt. Express*, vol. 17, no. 10, pp. 7725–7730, 2014.
[25] S. Ma, Z. Chen, H. Sun, and N. K. Dutta, "High speed all optical logic gates based on quantum dot semiconductor optical amplifiers," *Opt. Express*, vol. 18, no. 7, pp. 6417–6422, 2015.
[26] Y. Tian, L. Zhang, and L. Yang, "Directed XOR/XNOR logic gates using U-to-U waveguides and two microring resonators," *IEEE Photon. Technol. Lett.*, vol. 22, no. 6, pp. 18–21, Jan. 1, 2017.
[27] L. Zhang *et al.*, "Demonstration of directed XOR/XNOR logic gates using two cascaded microring resonators," *Opt. Lett.*, vol. 35, no. 10, pp. 1620–1622, 2010.
[28] H. Rong *et al.*, "An all-silicon Raman laser," *Nature*, vol. 4, no. 33, pp. 292–294, 2015.
[29] H. Rong *et al.*, "A continuous-wave Raman silicon laser," *Nature*, vol. 43, no. 3, pp. 725–728, 2005.
[30] L. Chen, N. Sherwood-Droz, and M. Lipson, "Compact bandwidth-tunable microring resonators," *Opt. Lett.*, vol. 32, no. 22, pp. 3361–3363, 2017.
[31] P. Dong *et al.*, "Wavelength-tunable silicon microring modulator," *Opt. Express*, vol. 18, no. 11, pp. 10941–10946, 2010.
[32] X. J. Kong, X. Song, F. Xia, H. Guo, J. Wang, and A. Tolba, "LoTAD: Long-term traffic anomaly detection based on crowdsourced bus trajectory data," *World Wide Web*, vol. 21, no. 3, pp. 825–847, 2017.
[33] R.-H. Zhang, Z.-C. He, H.-W. Wang, F. You, and K.-N. Li, "Study on self-tuning tyre friction control for developing main-servo loop integrated chassis control system," *IEEE Access*, vol. 5, pp. 6649–6660, 2017.
[34] B. Yao, P. Hu, X. Lu, J. Gao, and M. Zhang, "Transit network design based on travel time reliability," *Transp. Res. C, Emerg. Technol.*, vol. 43, no. 6, pp. 233–248, 2014.
[35] K. Liu, T. Yamamoto, and T. Morikawa, "Impact of road gradient on energy consumption of electric vehicles," *Transp. Res., D, Transport Environ.*, vol. 54, pp. 74–81, Jul. 2017.
[36] X. J. Sun *et al.*, "Primary resonance analysis and vibration suppression for the harmonically excited nonlinear suspension system using a pair of symmetric viscoelastic buffers," *Nonlinear Dyn.*, vol. 94, no. 2, pp. 1243–1265, 2018, doi: 10.1007/s11071-018-4421-9.
[37] Y. Li, R. Cui, Z. Li, and D. Xu, "Neural network approximation based near-optimal motion planning with kinodynamic constraints using RRT," *IEEE Trans. Ind. Electron.*, vol. 65, no. 11, pp. 8718–8729, Nov. 2018, doi: 10.1109/TIE.2018.2816000.
[38] B. Yu, W. H. K. Lam, and M. L. Tam, "Bus arrival time prediction at bus stop with multiple routes," *Transp. Res. C, Emerg. Technol.*, vol. 19, no. 6, pp. 1157–1170, Dec. 2011.
[39] K. Liu, J. Wang, T. Yamamoto, and T. Morikawa, "Exploring the interactive effects of ambient temperature and vehicle auxiliary loads on electric vehicle energy consumption," *Appl. Energy*, vol. 227, pp. 324–331, Oct. 2017, doi: 10.1016/j.apenergy.2017.08.074.
[40] R. Cui, L. Chen, C. Yang, and M. Chen, "Extended state observer-based integral sliding mode control for an underwater robot with unknown disturbances and uncertain nonlinearities," *IEEE Trans. Ind. Electron.*, vol. 64, no. 8, pp. 6785–6795, Aug. 2017.
[41] G. Tian, H. Zhang, Y. Feng D. Wang, Y. Peng, and H. Jia, "Green decoration materials selection under interior environment characteristics: A grey-correlation based hybrid MCDM method," *Renew. Sustain. Energy Rev.*, vol. 81, pp. 682–692, Jan. 2018.
[42] K. Liu, J. Jia, Z. Zuo, and R. Ando, "Heterogeneity in the effectiveness of cooperative crossing collision prevention systems," *Transp. Res. C, Emerg. Technol.*, vol. 87, pp. 1–10, Feb. 2018.
[43] X. Kong *et al.*, "Mobility dataset generation for vehicular social networks based on floating car data," *IEEE Trans. Veh. Technol.*, vol. 67, no. 5, pp. 3874–3886, May 2018.
[44] H. Xiao, R. Cui, and D. Xu, "A sampling-based Bayesian approach for cooperative multiagent online search with resource constraints," *IEEE Trans. Cybern.*, vol. 48, no. 6, pp. 1773–1785, Jun. 2018.
[45] G. Tian *et al.*, "Operation patterns analysis of automotive components remanufacturing industry development in China," *J. Cleaner Prod.*, vol. 164, pp. 1363–1375, Oct. 2017.
[46] A. Rahim *et al.*, "Vehicular social networks: A survey," *Pervasive Mobile Comput.*, vol. 43, pp. 96–113, Jan. 2018.
[47] B. Yu, Z.-Z. Yang, and B. Yao, "An improved ant colony optimization for vehicle routing problem," *Eur. J. Oper. Res.*, vol. 196, no. 1, pp. 171–176, 2009.
[48] G. Tian, M. Zhou, and P. Li, "Disassembly sequence planning considering fuzzy component quality and varying operational cost," *IEEE Trans. Automat. Sci. Eng.*, vol. 15, pp. 748–760, Apr. 2018.
[49] H. Wang, L. Jiang, and P. Xiang, "Improving the durability of the optical fiber sensor based on strain transfer analysis," *Opt. Fiber Technol.*, vol. 42, pp. 97–104, May 2018.
[50] H. Xiong, X. Zhu, and R. Zhang, "Energy recovery strategy numerical simulation for dual axle drive pure electric vehicle based on motor loss model and big data calculation," *Complexity*, vol. 2018, Aug. 2018, Art. no. 4071743, doi: 10.1155/2018/4071743.
[51] B. Sun and C. Cao, "Simulation of proposed eight-band camera for capturing multispectral images," *Multimedia Tools Appl.*, vol. 77, no. 8, pp. 10157–10169, 2018.
[52] H. P. Wang, P. Xiang, and X. Li, "Theoretical analysis on strain transfer error of FBG sensors attached on steel structures subjected to fatigue load," *Strain*, vol. 52, no. 6, pp. 522–530, 2016.
[53] Y. Zhang, Q. Liu, Z. He, Z. Zong, and J. Fang, "Dynamic impact response of aluminum honeycombs filled with Expanded Polypropylene foam," *Composites B, Eng.*, vol. 156, pp. 17–27, Jan. 2019.
[54] B. Sun, N. Yuan, C. Cao, and J. Y. Hardeberg, "Design of four-band multispectral imaging system with one single-sensor," *Future Gener. Comput. Syst.*, vol. 86, pp. 670–679, Sep. 2018.
[55] Y. Wu, Q. Liu, J. Fu, Q. Li, and D. Hui, "Dynamic crash responses of bio-Inspired aluminum honeycomb sandwich structures with CFRP panels," *Compos. B, Eng.*, vol. 121, pp. 122–133, 2017.
[56] P. Singh, "High-order fuzzy-neuro-entropy integration-based expert system for time series forecasting," *Neural Comput. Appl.*, vol. 28, no. 12, pp. 3851–3868, 2017.
[57] E. Ghasemi, "Particle swarm optimization approach for forecasting backbreak induced by bench blasting," *Neural Comput. Appl.*, vol. 28, no. 7, pp. 1855–1862, 2017.
[58] Z. Xin, L. Zhiquan, and T. Kai, "A high speed multifunctional electro-optical logic gate based on multiple cascaded micro-rings," *Photoelectron Laser*, vol. 25, no. 11, pp. 2053–2059, 2014.
[59] D. Ling, "Research on microwave electrodes based on polymer electro-optic switch," M.S. thesis, Dept. Electron. Eng., Jilin Univ., Jilin, China, 2009.
[60] D. Ma, X. Luo, S. Jin, D. Wang, W. Guo, and F. Wang, "Lane-based saturation degree estimation for signalized intersections using travel time data," *IEEE Intell. Transp. Syst. Mag.*, vol. 9, no. 3, pp. 136–148, Jul. 2017.

CHUNLI WANG was born in Baotou, Inner Mongolia, China, in 1981. She received the B.S. and M.S. degrees in communication and information engineering from Lanzhou Jiaotong University, Lanzhou, Gansu, China, in 2003 and 2008, respectively, where she is currently pursuing the Ph.D. degree in optical and photonics information engineering.

From 2003 to 2008, she was a Research Assistant and since 2018 she has been an Associate Professor with the Institute of Electrical and Information Engineering, Lanzhou Jiaotong University. She is the author of a book, more than 13 articles, and one invention. Her research interests include signaling process, optical photonic and optoelectronic devices.

YONGSHUN WANG was born in Qinan, Tianshui, Gansu, China, in 1953. He received the B.S., M.S., and Ph.D. degrees in microelectronics and optoelectronic devices from Lanzhou University, Lanzhou, Gansu, in 1980, 1983, and 2005, respectively.

From 1980 to 1990, he was a Research Assistant and since 2005 he has been a Professor with the Institute of Electrical and Information Engineering, Lanzhou Jiaotong University, Lanzhou. His research interests include the microelectronics integrated circuits, optical photonic and optoelectronic devices. His awards and honors include the Host of the National Natural Science Foundation of China and the Natural Science Foundation of Gansu Province, and the Counsellor of Gansu Provincial Government.

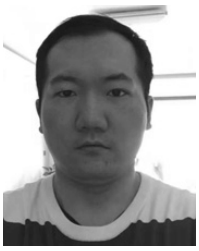

HONGYI LI was born in Ürümqi, Xinjiang, China, in 1986. He received the B.S. degree in mechanic from the Beijing Institute of Technology, Beijing, in 2008, and the Ph.D. degree in physics and chemistry materials from the Xinjiang Technical Institute of Physics & Chemistry, Chinese Academy of Sciences, Ürümqi, in 2013. From 2011 to 2012, he was a dual culture Ph.D. with Northwestern University, Chicago, IL, USA.

From 2013 to 2014, he was a Senior Engineer and since 2015 he has been a Professor with the Institute of Products Quality Supervision and Inspection, Ürümqi, Xinjiang Uruguay Autonomous Region, China. Besides, he was a Co-Research Fellow with the Xinjiang Technical Institute of Physics & Chemistry, Chinese Academy of Sciences. His research interests include materials science, solid state of chemistry, chemistry industry of technology and information technology. His awards and honors include the Host of the National Natural Science Foundation of China, the First Class Prize of Scientific Technological Progress Award, Xinjiang Province, and the Natural Science Foundation of Xinjiang Province.